Volume 3 | Number 18 | 14 May 2015 | Pages 4587–4830

Journal of Materials Chemistry C

Materials for optical, magnetic and electronic devices

www.rsc.org/MaterialsC

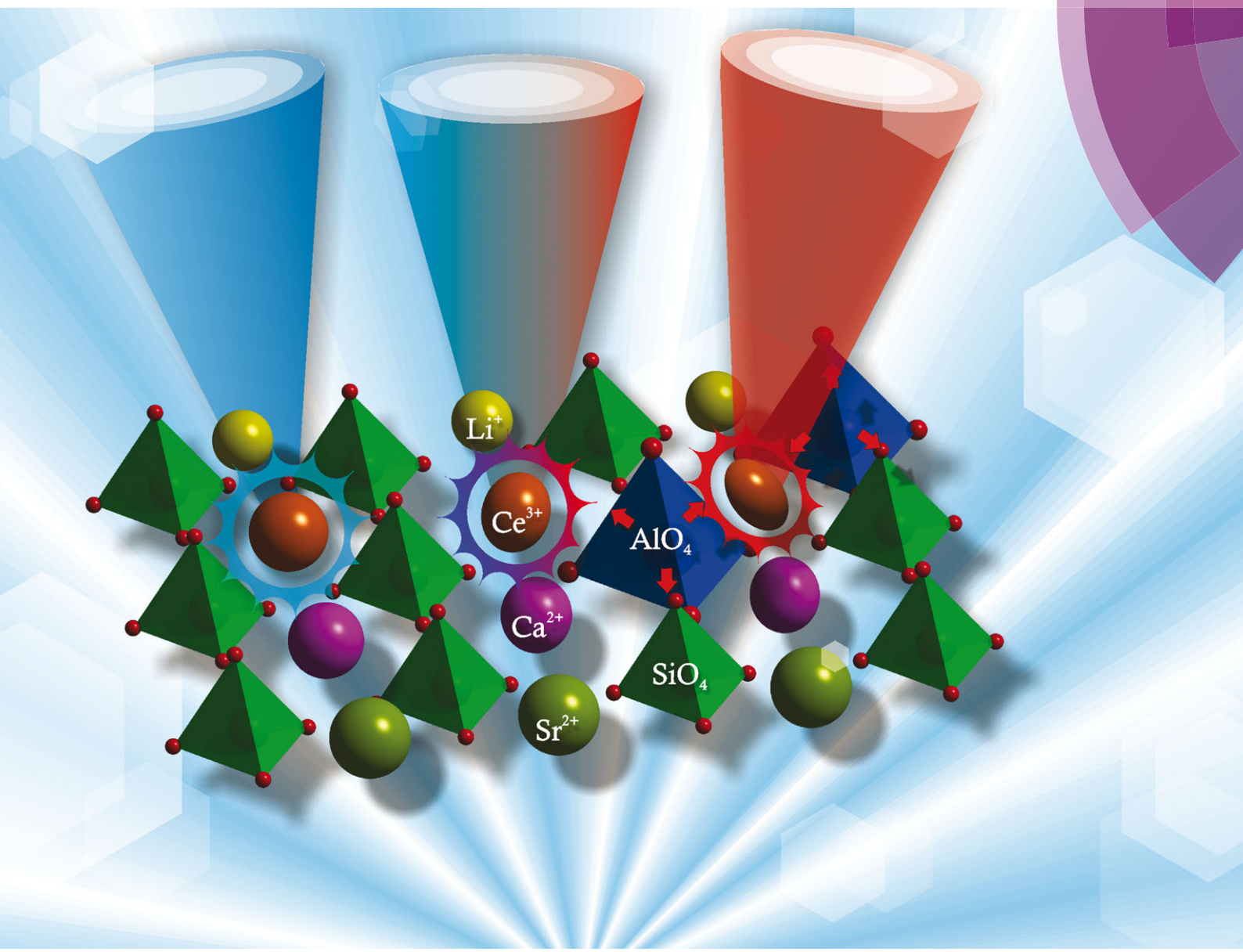

ISSN 2050-7526

ROYAL SOCIETY OF CHEMISTRY

PAPER

Zhiguo Xia *et al.*

Effect of Al/Si substitution on the structure and luminescence properties of $CaSrSiO_4:Ce^{3+}$ phosphors: analysis based on the polyhedra distortion

Journal of Materials Chemistry C

PAPER

View Article Online
View Journal | View Issue

Cite this: J. Mater. Chem. C, 2015, 3, 4616

Effect of Al/Si substitution on the structure and luminescence properties of $CaSrSiO_4:Ce^{3+}$ phosphors: analysis based on the polyhedra distortion†

Shihai Miao,[a] Zhiguo Xia,*[ab] Maxim S. Molokeev,[cd] Mingyue Chen,[b] Jie Zhang[a] and Quanlin Liu[b]

Received 3rd February 2015,
Accepted 24th March 2015

DOI: 10.1039/c5tc00339c

www.rsc.org/MaterialsC

Blue-emitting $CaSrSiO_4:Ce^{3+},Li^+$ phosphors were prepared by a high temperature solid-state method, and the effect of substituting Al^{3+} for Si^{4+} in $CaSrSiO_4:Ce^{3+},Li^+$ has been studied. Crystal structures of the as-prepared $Ca_{1-y}Sr_{1-y}Si_{1-x}Al_xO_4:yCe^{3+},yLi^+$ phosphors were resolved by the Rietveld method, which suggested that all the samples belonged to the orthorhombic symmetry (*Pnma*) group of α-$CaSrSiO_4$. The photoluminescence (PL) emission and excitation spectra, the lifetime, and the effect of Al^{3+} concentration on the PL properties were investigated in detail. The emission peaks of the $CaSrSi_{1-x}Al_xO_4:Ce^{3+},Li^+$ (x = 0–0.10) phosphors were red-shifted from 452 to 472 nm with increasing Al/Si ratio. The red-shift of the Ce^{3+} emission is ascribed to the polyhedra distortion of the cations, originating from the variation in the neighboring $[(Si,Al)O_4]$ polyhedra, and the detailed mechanism has been discussed.

1. Introduction

Solid-state white lighting with superior efficiency, longer duration times, and tunable optical performances is in the process of replacing traditional fluorescent and incandescent light sources. Among them, phosphor converted light emitting diodes (pc-LEDs) have been widely studied and applied as a fourth-generation light source.[1–4] Yellow-emitting phosphor $Y_3Al_5O_{12}:Ce^{3+}$ (YAG:Ce) in combination with a blue InGaN LED chip for white LEDs has become main stream. Apart from the well-known YAG:Ce system, some other matrices can also act as excellent phosphor hosts, such as nitrides/oxynitrides, silicates/borates, molybdates/tungstates, and so on, which show excellent photoluminescence (PL) properties.[5–8] The silicate phosphors, represented by Eu^{2+} or Ce^{3+} doped orthosilicates A_2SiO_4 (A = Ca, Sr, Ba), have drawn much attention owing to their broad excitation/emission bands, tunable optical properties, moderate synthesis methods and low fabrication costs.[9]

Based on a review of the recent papers on the main research topics and the important considerations in the design of new orthosilicate phosphors, there are three aspects that need to be developed in the future.[9–15] One is that the nitridation of orthosilicate phosphors can induce a red-shift of the emission peaks. For example, Park reported red-emitting phosphors $Sr_{2-y-z}Ca_zSi(O_{1-x}N_x)_4:yEu^{2+}$, and the nitridation effect led to a dramatic change in the crystal field.[11] Black found new orange–red-emitting Eu^{2+}/Ce^{3+} doped $LaBaSiO_3N$ and $LaSrSiO_3N$ phosphors with β-K_2SiO_4 structures.[12] Another aspect is the design of the donor–acceptor couple in the A_2SiO_4 phase, and tunable emission can occur *via* the energy transfer of the codoped ions. Examples include the full-color emitting phosphors $Ba_{1.3}Ca_{0.7}SiO_4:Eu^{2+},Mn^{2+}$ and $Ba_{1.55}Ca_{0.45}SiO_4:Eu^{2+},Mn^{2+}$.[13,14] The last aspect is the exploration of A_2SiO_4-based phosphors *via* composition optimization and structural modification. Cheetham's group carefully investigated the phase relationship of Ca_2SiO_4 and found a suitable way to stabilize the γ-Ca_2SiO_4 phase and develop yellow emitting phosphors for pc-LEDs.[3] Seshadri's group reported $Sr_xBa_{2-x}SiO_4:Eu^{2+}$ phosphors, and the intermediate composition with 46% Sr had the optimum luminescence properties.[15]

As far as we know, the luminescence properties of Ce^{3+} doped $CaSrSiO_4$ have not been reported. As mentioned above, the intermediate compositions in the M_2SiO_4 phase provide

[a] School of Materials Sciences and Technology, China University of Geosciences, Beijing 100083, China
[b] School of Materials Sciences and Engineering, University of Science and Technology Beijing, Beijing 100083, China. E-mail: xiazg@ustb.edu.cn; Fax: +86-10-8237-7955; Tel: +86-10-8237-7955
[c] Laboratory of Crystal Physics, Kirensky Institute of Physics, SB RAS, Krasnoyarsk 660036, Russia
[d] Department of Physics, Far Eastern State Transport University, Khabarovsk, 680021 Russia

† Electronic supplementary information (ESI) available: The fractional atomic coordinates and isotropic displacement parameters (Å^2) and the corresponding crystallographic information files (CIF) of $(Ca_{0.95}Sr_{0.95}Ce_{0.05}Li_{0.05})(Si_{1-x}Al_x)O_4$ (x = 0, 0.01 and 0.1). See DOI: 10.1039/c5tc00339c

some opportunities to search for new phosphors. In this work, we studied the luminescence properties of blue-emitting $CaSrSiO_4$:Ce^{3+},Li^+ phosphors, and the effect of substituting Al^{3+} for Si^{4+} in $CaSrSiO_4$:Ce^{3+},Li^+ has also been studied. The crystal structures and luminescence properties of $CaSrSi_{1-x}Al_xO_4$:Ce^{3+},Li^+ (x = 0–0.10) phosphors with increasing Al/Si ratio have been discussed, and the observed red-shift is ascribed to the polyhedra distortion of cations occupied by Ce^{3+}.

2. Experimental

The designed $Ca_{1-y}Sr_{1-y}Si_{1-x}Al_xO_4$:$yCe^{3+}$,$yLi^+$ phosphors were synthesized by a conventional high temperature solid-state reaction. The starting materials were as follows: $SrCO_3$ (A.R.), $CaCO_3$ (A.R.), Li_2CO_3 (A.R.), SiO_2 (A.R.), Al_2O_3 (A.R.) and CeO_2 (99.99%). After mixing and grinding in an agate mortar for 25 min, the mixture was placed in a crucible and then sintered at 1400 °C for 5 h in a reducing atmosphere of H_2 (10%) and N_2 (90%) to produce the final samples. Finally, the prepared phosphors were cooled to room temperature and reground for further measurements.

Powder X-ray diffraction (XRD) measurements were performed on a D8 Advance diffractometer (Bruker Corporation, Germany), operating at 40 kV and 40 mA with Cu Kα radiation (λ = 1.5406 Å). The scanning rate for phase identification was fixed at 4° min^{-1} with a 2θ range from 10° to 70°, and the data for the Rietveld analysis were collected in a step-scanning mode with a step size of 0.02° and 10 s counting time per step over a 2θ range from 10° to 120°. The PL and photoluminescence excitation (PLE) spectra were recorded by a Hitachi F-4600 spectrophotometer equipped with a 150 W xenon lamp as the excitation source. The decay curves were recorded on an Edinburgh Instrument (FLSP920) with a nF900 flash lamp as the excitation source. The quantum efficiency was measured using an integrating sphere on the same FLSP920 fluorescence spectrophotometer.

3. Results and discussion

XRD patterns of all the as-prepared $Ca_{0.95}Sr_{0.95}Si_{1-x}Al_xO_4$:$0.05Ce^{3+}$,$0.05Li^+$ (x = 0, 0.1, 0.2, 0.3, 0.4, 0.5, 0.7 and 0.8) phosphors are given in Fig. 1a. Although the designed chemical formula did not fulfil the charge balance, this may be overcome with some vacancies (point defects) in the oxygen lattice. The standard data for $CaSrSiO_4$ (JCPDS 72-2260) is also shown as a reference in Fig. 1a. The magnified XRD patterns between 31° and 34° are shown in Fig. 1b. By comparing the diffraction peaks in Fig. 1, we can see that the obtained samples can be indexed to the $CaSrSiO_4$ phase (JCPDS 72-2260) when $x \leq 0.1$. Some diffraction peaks ascribed to the impurity appear in the vicinity of 33° when the doping amount of Al^{3+} is more than x = 0.1, therefore the maximum dissolution amount of Al substituted Si in the $CaSrSiO_4$ host should be below x = 0.1.

In order to further investigate the phase formation depending on the Al/Si substitution of the $Ca_{0.95}Sr_{0.95}Si_{1-x}Al_xO_4$:$0.05Ce^{3+}$,$0.05Li^+$ phosphors, XRD patterns for the selected samples with different Al/Si substitution amounts of x = 0.01 and x = 0.1 were measured and are shown in Fig. 2a. The three samples shown in Fig. 2a clearly indicate that all the diffraction peaks of the selected samples agree well with the standard data for the orthorhombic phase of $CaSrSiO_4$ (JCPDS 72-2260), suggesting that they belong to the pure phase, as mentioned in Fig. 1. Accordingly, the powder diffraction data of $(Ca_{0.95}Sr_{0.95}Ce_{0.05}Li_{0.05})(Si_{1-x}Al_x)O_4$ (x = 0, 0.01 and 0.1) were then refined *via* the Rietveld analysis performed by using TOPAS 4.2. The Rietveld plots for the three samples are shown in Fig. 2b, c and d, respectively, and the main parameters of the processing and refinement are listed in Table 1. As shown in Fig. 2b–d, almost all the peaks could be

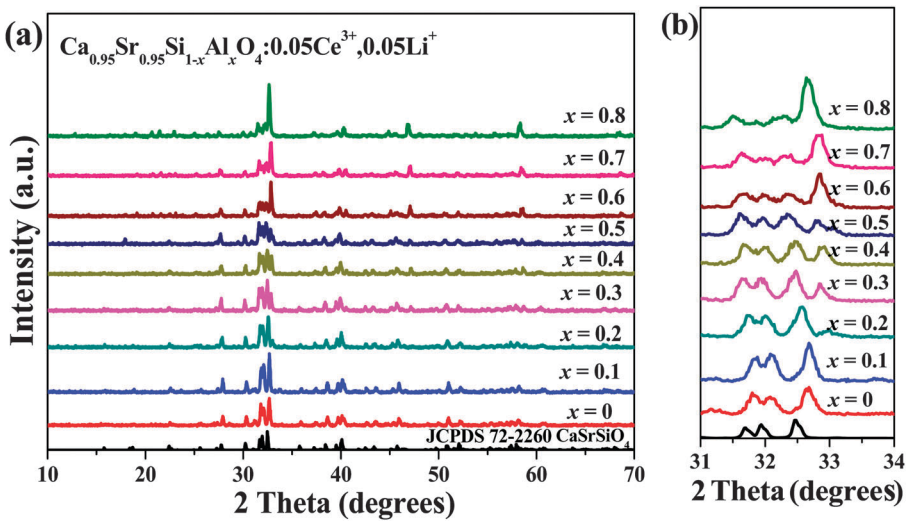

Fig. 1 XRD patterns (a) and magnified patterns between 31° and 34° (b) of $Ca_{0.95}Sr_{0.95}Si_{1-x}Al_xO_4$:$0.05Ce^{3+}$,$0.05Li^+$. The standard data for $CaSrSiO_4$ (JCPDS 72-2260) is shown as a reference.

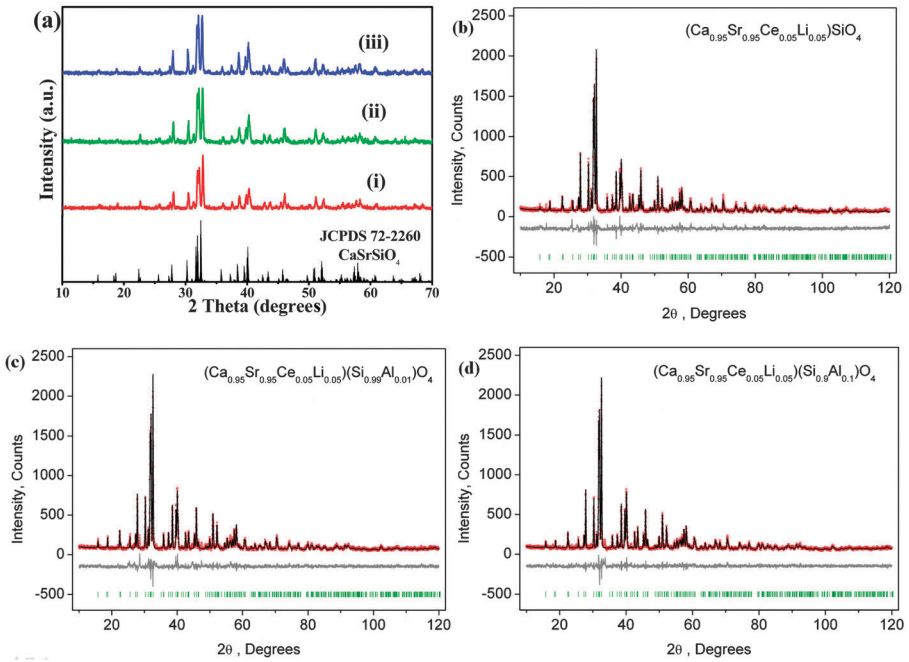

Fig. 2 (a) XRD patterns of $Ca_{0.95}Sr_{0.95}SiO_4$:0.05Ce^{3+},0.05Li^+ (i), $Ca_{0.95}Sr_{0.95}Si_{0.99}Al_{0.01}O_4$:0.05$Ce^{3+}$,0.05$Li^+$ (ii), and $Ca_{0.95}Sr_{0.95}Si_{0.9}Al_{0.1}O_4$:0.05$Ce^{3+}$,0.05$Li^+$ (iii). The standard data for $CaSrSiO_4$ (JCPDS 72-2260) is shown as a reference. (b) Difference Rietveld plot of $(Ca_{0.95}Sr_{0.95}Ce_{0.05}Li_{0.05})(Si_{1-x}Al_x)O_4$, x = 0. (c) Difference Rietveld plot of $(Ca_{0.95}Sr_{0.95}Ce_{0.05}Li_{0.05})(Si_{1-x}Al_x)O_4$, x = 0.01. (d) Difference Rietveld plot of $(Ca_{0.95}Sr_{0.95}Ce_{0.05}Li_{0.05})(Si_{1-x}Al_x)O_4$, x = 0.1.

Table 1 Main parameters of the processing and refinement of the $(Ca_{0.95}Sr_{0.95}Ce_{0.05}Li_{0.05})(Si_{1-x}Al_x)O_4$ (x = 0, 0.01 and 0.1) samples

	Compound		
	x = 0	x = 0.01	x = 0.1
Space group	*Pnma*	*Pnma*	*Pnma*
a/Å	6.9541(4)	6.9527(3)	6.9490(3)
b/Å	5.5826(3)	5.5872(3)	5.5922(3)
c/Å	9.4520(5)	9.4552(5)	9.4653(4)
V/Å^3	366.95(3)	367.30(3)	367.83(3)
Z	8	8	8
2θ-interval/°	5–120	5–120	5–120
No. reflections	309	309	309
No. refinement parameters	44	44	44
R_{wp}/%	14.24	12.59	11.54
R_p/%	10.27	9.52	8.80
R_{exp}/%	9.72	9.41	9.54
χ^2	1.46	1.34	1.21
R_B/%	4.66	3.44	2.73

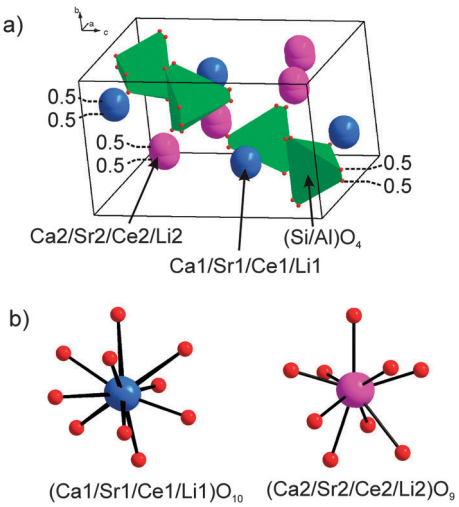

Fig. 3 (a) Crystal structure of $(Ca_{0.95}Sr_{0.95}Ce_{0.05}Li_{0.05})(Si_{1-x}Al_x)O_4$; (b) coordination of Ca1/Sr1 and Ca2/Sr2 ions doped with Ce^{3+} and Li^+.

indexed to the orthorhombic cell (*Pnma*) with parameters close to α-$CaSrSiO_4$. Therefore, the crystal structure of $CaSrSiO_4$ was taken as a starting model for the Rietveld refinement. Fig. 3 demonstrates the representative crystal structure of $(Ca_{0.95}Sr_{0.95}Ce_{0.05}Li_{0.05})(Si_{1-x}Al_x)O_4$ and the coordination environment of the Ca1/Sr1 and Ca2/Sr2 ions doped with Ce^{3+} and Li^+. As far as we know, there are two Ca/Sr sites in the $CaSrSiO_4$ structure with different coordination numbers – a 10-coordinate Ca1/Sr1 site and a 9-coordinated Ca2/Sr2 site – and each of them is disordered by Ca/Sr with an occupancy of $\frac{1}{2}$. The same model was realized in our model for the study of $(Ca_{0.95}Sr_{0.95}Ce_{0.05}Li_{0.05})(Si_{1-x}Al_x)O_4$, and the Ca/Sr occupations were also refined, but the sum of their occupations was equal to 0.475 instead of 0.5 because Ce^{3+} and Li^+ ions also existed in these sites with occupancies of 0.0125 and 0.0125, respectively. Based on the above crystal structure analysis, refinement in such a model was stable and gave low R-factors (Table 1 and Fig. 2b–d), suggesting that the phase structures were invariable with the introduction of Al. The cell volume of the compound with x = 0.1 was bigger than the cell volumes of the compounds with x = 0.01 and x = 0, which is in accordance with the bigger ion radius (IR) of Al^{3+} (CN = 4, IR = 0.39 Å) in comparison with the IR of Si^{4+} (CN = 4, IR = 0.26 Å).[16] The fractional atomic coordinates and isotropic

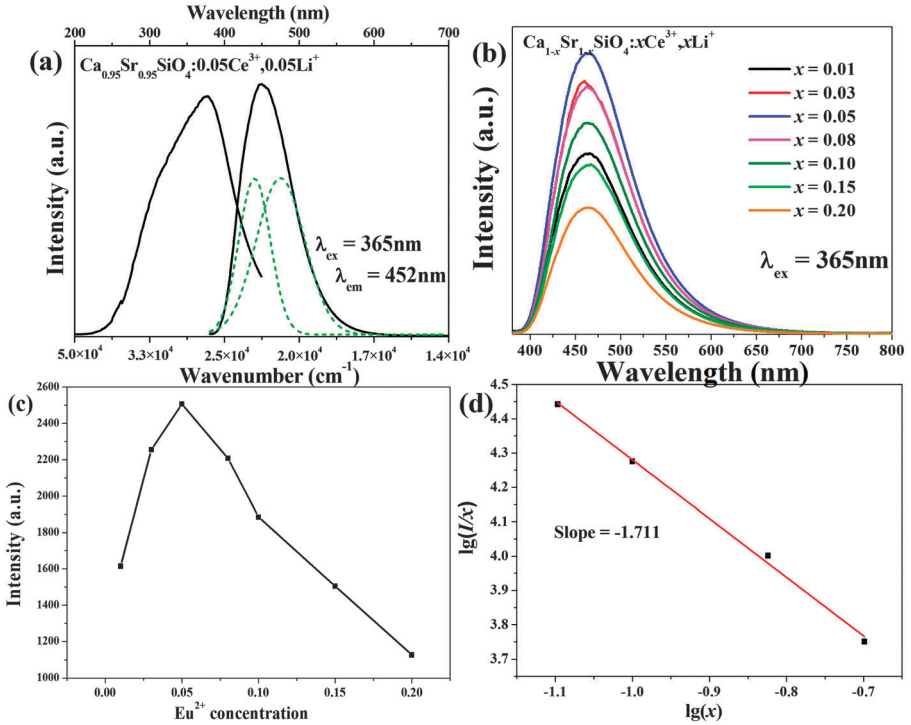

Fig. 4 (a) PLE and PL spectra of $Ca_{0.95}Sr_{0.95}SiO_4$:0.05Ce^{3+},0.05Li^+ and the Gaussian fitting of the PL spectrum, (b) PL spectra of $Ca_{1-x}Sr_{1-x}SiO_4$:*x*-Ce^{3+},*x*Li^+ (*x* = 0.01, 0.03, 0.05, 0.08 and 0.10). (c) The PL intensity of the plot of $Ca_{1-2x}SrSiO_4$:*x*Ce^{3+},*x*Li^+ as a function of Ce^{3+} content. (d) The relationship of lg(*x*) *versus* lg(*I*/*x*).

displacement parameters (Å^2) of $(Ca_{0.95}Sr_{0.95}Ce_{0.05}Li_{0.05})(Si_{1-x}Al_x)O_4$ (*x* = 0, 0.01 and 0.1) are given in Table S1 (ESI†), and the corresponding crystallographic information files (CIF) are also presented in the ESI.†

The PL and PLE spectra of $Ca_{0.95}Sr_{0.95}SiO_4$:0.05Ce^{3+},0.05Li^+ are shown in Fig. 4a. The PLE spectrum monitored at 452 nm exhibits a broad band from 200 to 450 nm, indicating a complex splitting of the $5d^1$ excited state of Ce^{3+}. The emission spectrum shows a broad band centered at 452 nm when excited at 365 nm. Based on the Gaussian fitting, the PL spectrum in Fig. 4a could be divided into two Gaussian peaks at 440 nm (22 727 cm^{-1}) and 475 nm (21 053 cm^{-1}), and the energy difference was calculated to be 1673 cm^{-1}, which showed a difference compared with the theoretical value of 2000 cm^{-1} for the $^2F_{7/2}$ and $^2F_{5/2}$ states of Ce^{3+}. Therefore, we proposed that Ce/Li are located as two kinds of Ca/Sr sites and eventually two kinds of luminescent centers are formed. Moreover, the emission positions of the Ce^{3+} ion are strongly dependent on its local environment. It has been suggested that it obeys an empirical relationship between the energetic position of the Ce^{3+} emission and the local structure in various compounds. The equation is given as follows:[17]

$$E = Q\left[1 - \left(\frac{V}{4}\right)^{\frac{1}{V}} 10^{-\frac{n \times E_a \times r}{80}}\right] \quad (1)$$

where *E* represents the real position of the d-band edge in energy for Ce^{3+} (cm^{-1}), *Q* is the position in energy for the lower d-band edge for the Ce^{3+} free ions, *V* is the valence of the Ce^{3+} ion, *n* is the number of anions in the immediate shell about this ion, *r* is the radius of the host cation replaced by the Ce^{3+} ion (Å), and E_a is the electron affinity of the atoms that form anions. In the present case, there are two Ca/Sr sites in the $CaSrSiO_4$ structure. Therefore, most parameters were invariable in eqn (1), so that the coordination number *n* is proportional to the observed position of the d-band edge for Ce^{3+}. As a result, the Ce^{3+} center showing an emission peak at 440 nm occupied the 10-coordinate Ca^{2+}/Sr^{2+} site, and the other Ce^{3+} center showing an emission at 475 nm was related to the 9-coordinate Ca^{2+}/Sr^{2+} site.

The influence of the polyhedron on the crystal field splitting can be denoted by the ε_{cfs} value.[18,19] A large ε_{cfs} value is the main reason for the large red shift of the first f–d transition, and there is an empirical relationship between the ε_{cfs} value and the average distance (*R*) between the activator and the neighboring anions:

$$\varepsilon_{cfs} = \beta_{poly}^{Q} R_{av}^{-2} \quad (2)$$

where R_{av} is close to the average distance between the anions and cations that are replaced by Ce^{3+}, β_{poly} is a constant that depends on the type of coordinating polyhedron and *Q* is 3 for Ce^{3+}. ε_{cfs} is likely to decrease with the increase in coordination number and the average distance (*R*).

Except for the crystal field splitting, the centroid shift also influences the energy of the lowest excited 5d level. The 5d

centroid shift for Ce^{3+} can be expressed by the following equation:

$$\varepsilon_c = A\sum_{i=1}^{N}\frac{\alpha_{SP}^{i}}{(R_i - 0.6\Delta R)^6} \quad (3)$$

where R_i is the distance (pm) between Ce^{3+} and anion i in the undistorted lattice, the summation is over all O anions that coordinate Ce^{3+}, $0.6\Delta R$ is a correction for the lattice relaxation around Ce^{3+}, ΔR is the difference between the radii of Ce^{3+} and Ca^{2+}/Sr^{2+} in different sites, α_{sp}^{i} (10^{-30} m^{-3}) is the spectroscopic polarizability of anion i, and A is a constant (1.79×10^{13}). The value of ε_c for Ce^{3+} in Ca1/Sr1 (ten-coordinate) is smaller than the value for Ce^{3+} in Ca2/Sr2 (nine-coordinate), by introducing the values of N, R_i and ΔR.[18,19]

Fig. 4b gives the PL spectra of $Ca_{1-x}Sr_{1-x}SiO_4$:xCe^{3+},xLi^+ (x = 0.01, 0.03, 0.05, 0.08, 0.10, 0.15 and 0.20). Owing to the 5d–4f allowed transition of Ce^{3+}, the emission spectra consist of an asymmetric broad band centered at 452 nm. The emission intensities have an increasing trend with increasing Ce^{3+} concentration, maximizing at x = 0.05, and then decrease, which could be attributed to the internal concentration quenching effect. Also, from the PL intensities as a function of Ce^{3+} content (Fig. 4c), we can conclude that the quenching concentration of Ce^{3+} appears at x = 0.05. Non-radiative energy transfer between different Ce^{3+} ions may occur by exchange interactions, radiation reabsorption, or multipole–multipole interactions. The critical energy transfer distance between Ce^{3+} ions can be calculated by using the concentration quench eqn (4), proposed by Blasse:[20]

$$R_c \approx 2\left(\frac{3V}{4\pi x_c N}\right)^{\frac{1}{3}} \quad (4)$$

where V is the volume of the unit cell, x_c is the critical concentration, N is the number of cations in the unit cell and V is the volume of the unit cell. V = 366.95 Å^3, N = 8 and x_c = 0.05 for $Ca_{1-x}Sr_{1-x}SiO_4$:xCe^{3+},xLi^+. According to the above equation, the critical distance for the energy transfer is estimated to be about 12.05 Å. Therefore, according to the Dexter theory, the non-radiative transitions between Eu^{2+} ions take place *via* electric multipolar interactions.[21] The interaction type between sensitizers or between a sensitizer and activator can be calculated by the following equation:[22,23]

$$\frac{I}{x} = K\left[1 + \beta(x)^{\theta/3}\right]^{-1} \quad (5)$$

where I is the emission intensity, x is the concentration of the activator ions beyond the critical concentration of x = 0.05, β and K are constants under the same excitation conditions, and θ is an indication of the electric multipolar character. Based on the previous report,[23] θ = 3 for the energy transfer among the nearest-neighbor ions, while θ = 6, 8 and 10 for dipole–dipole (d–d), dipole–quadrupole (d–q), and quadrupole–quadrupole (q–q) interactions, respectively. In order to obtain a correct value of θ for the emission centers, the dependence of lg(I/x) on lg(x) was investigated and it yielded a straight line with a slope equal to $-\theta/3$. The fitting plot for the Ce^{3+} emission centers corresponding to the concentrations above the Ce^{3+} quenching concentration is shown in Fig. 4d. The slope is -1.711, and the value of θ can be calculated as 5.133, which is closest to 6. This result verified that the concentration quenching in $Ca_{1-x}Sr_{1-x}SiO_4$:xCe^{3+},xLi^+ phosphors is ascribed to dipole–dipole interactions.[24]

As reported previously, the addition of Al in the Ca_2SiO_4 host can stabilize the γ-Ca_2SiO_4 phase and change the emission colors of Ce^{3+} in the studied host owing to the formation of new polymorphs.[3] The PLE and PL spectra of $Ca_{0.95}Sr_{0.95}Si_{0.9}Al_{0.1}O_4$:$0.05Ce^{3+}$,$0.05Li^+$ are given in Fig. 5a. The excitation spectrum is similar to that of $Ca_{0.95}Sr_{0.95}SiO_4$:$0.05Ce^{3+}$,$0.05Li^+$ with a broad band. Under 365 nm UV light excitation, the $Ca_{0.95}Sr_{0.95}Si_{0.9}Al_{0.1}O_4$:$0.05Ce^{3+}$,$0.05Li^+$ phosphor showed an emission band ranging from 400 to 600 nm with a maximum intensity at 472 nm. Compared to the emission spectrum of the $Ca_{0.95}Sr_{0.95}SiO_4$:$0.05Ce^{3+}$,$0.05Li^+$ phosphor, we found an apparent red shift owing to the Al/Si substitution even if the phase structure was invariable, as discussed above. Therefore, the effect of Al/Si substitution on the luminescence properties of $Ca_{0.95}Sr_{0.95}SiO_4$:$0.05Ce^{3+}$,$0.05Li^+$ phosphors was studied, and the doped Ce^{3+} concentration was fixed at 0.05. The as-measured and normalized emission spectra for the $Ca_{0.95}Sr_{0.95}Si_{1-x}Al_xO_4$:$0.05Ce^{3+}$,$0.05Li^+$ (x = 0, 0.01, 0.03, 0.05, 0.08 and 0.10) phosphors under UV excitation (λ_{ex} = 365 nm) are shown in Fig. 5b and c, respectively. As shown in Fig. 5b, the emission intensities decrease sharply with the introduction of Al, however, it was nearly invariable in the range of x = 0.01–0.1. From Fig. 5c we can see that the emission spectra gradually shift in the long wavelength direction from 452 nm to 472 nm (red shift) with increasing Al/Si ratios. We also measured the internal quantum efficiency (QE) of the selected $Ca_{0.95}Sr_{0.95}Si_{1-x}Al_xO_4$:$0.05Ce^{3+}$,$0.05Li^+$ (x = 0, 0.01, 0.1) phosphors. The measured QEs of the $Ca_{0.95}Sr_{0.95}Si_{1-x}Al_xO_4$:$0.05Ce^{3+}$,$0.05Li^+$ (x = 0, 0.01, 0.1) phosphors were determined as 10.0%, 39.2%, and 53.1%, respectively. It is believed that the QE can be further improved through optimization of the processing conditions in the future.

To study the dynamics of the luminescence, we measured the PL decay curves of the Ce^{3+} emission in the $Ca_{0.95}Sr_{0.95}Si_{1-x}Al_xO_4$:$0.05Ce^{3+}$,$0.05Li^+$ phosphors. As depicted in Fig. 5d, one can see that the decay curves of the Ce^{3+} emission in the $Ca_{0.95}Sr_{0.95}Si_{1-x}Al_xO_4$:$0.05Ce^{3+}$,$0.05Li^+$ phosphors all obey a second-order exponential decay, which can be fitted using this formula:[25,26]

$$I(t) = I_0 + A_1\exp(-t/\tau_1) + A_2\exp(-t/\tau_2) \quad (6)$$

where t is the time, τ_1 and τ_2 are the rapid and slow times for the exponential components, A_2 and A_1 are constants, and $I(t)$ is the luminescence intensity at time t. We can then obtain the average lifetime, τ^*, by using the following equation:

$$\tau^* = (A_1\tau_1^{\,2} + A_2\tau_2^{\,2})/(A_1\tau_1 + A_2\tau_2) \quad (7)$$

The calculated average decay lifetimes of the Ce^{3+} ions in the $Ca_{0.95}Sr_{0.95}Si_{1-x}Al_xO_4$:$0.05Ce^{3+}$,$0.05Li^+$ phosphors (x = 0, 0.01, 0.05, 0.10) were determined to be 39.9, 40.2, 41.4, and 42.5 ns, respectively. We can see that the lifetime values slightly increase, but on the whole there is no obvious change.[27,28]

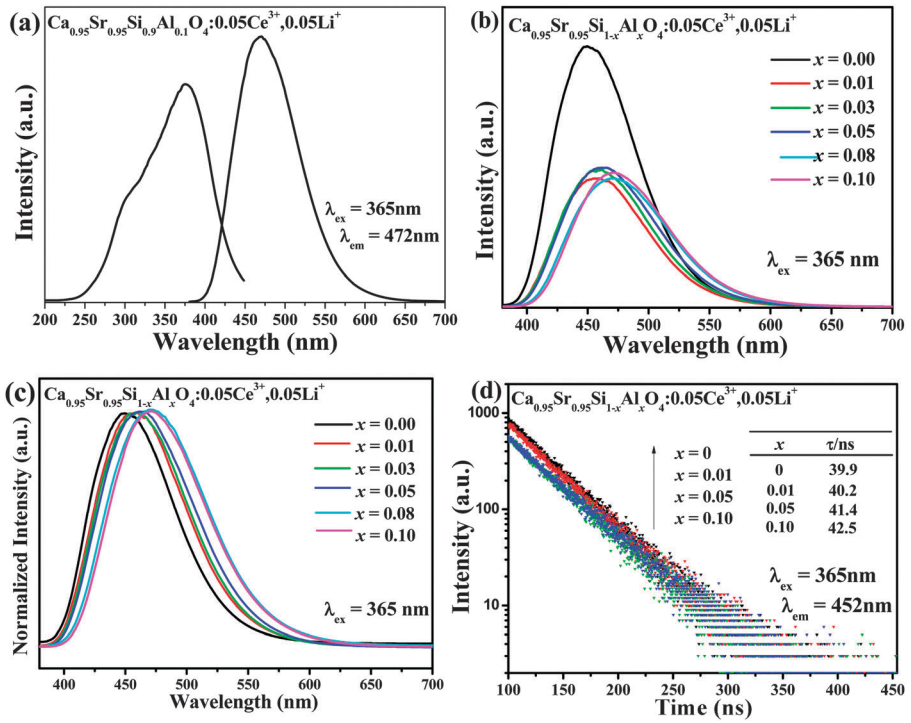

Fig. 5 (a) PLE and PL spectra of $Ca_{0.95}Sr_{0.95}Si_{0.9}Al_{0.1}O_4$:0.05$Ce^{3+}$,0.05$Li^+$, (b) PL spectra of $Ca_{0.95}Sr_{0.95}Si_{1-x}Al_xO_4$:x$Ce^{3+}$,x$Li^+$ (x = 0, 0.01, 0.03, 0.05, 0.08 and 0.10), (c) the normalized PL spectra, (d) decay curves of the Ce^{3+} emission in the $Ca_{0.95}Sr_{0.95}Si_{1-x}Al_xO_4$:0.05$Ce^{3+}$,0.05$Li^+$ phosphors under excitation at 365 nm, monitored at 452 nm.

Although the phase structures of $Ca_{0.95}Sr_{0.95}Si_{1-x}Al_xO_4$:0.05$Ce^{3+}$,0.05$Li^+$ are invariable with Al/Si substitution, the emission peaks are red shifted, suggesting that the local structures changed. Since the dopant Ce^{3+} will occupy the Ca/Sr cation sites, the crystal structures of the investigated compounds consist of disordered $(Si,Al)O_4$ tetrahedra and two types of cation polyhedra: $(Ca1/Sr1/Ce1/Li1)O_{10}$ and $(Ca2/Sr2/Ce2/Li2)O_9$, as shown in Fig. 3. Distortion of the $(Ca1/Sr1/Ce1/Li1)O_{10}$ and $(Ca2/Sr2/Ce2/Li2)O_9$ polyhedra are linked to the increase in the average Al/Si ion size with increasing x. Calculations prove that the average bond length (Al/Si–O) increases from 1.625 to 1.626 Å to 1.643 Å with increasing x from 0, to 0.01 to 0.1. Since $(Ca1/Sr1/Ce1/Li1)O_{10}$ and $(Ca2/Sr2/Ce2/Li2)O_9$ polyhedra connect with some $(Al/Si)O_4$ tetrahedra by edges and faces, increasing the $(Al/Si)O_4$ size leads to increasing some O–(Ca/Sr/Ce/Li)–O angles and of course this distorts the polyhedra. The $(Al/Si)O_4$ tetrahedra, which connect with polyhedra only by nodes, also distort due to d(Al/Si–O) enlarging but d(Ca/Sr/Ce/Li–O) shortening. Fig. 6 shows the schematic diagram of the polyhedra distortion for $(Ca1/Sr1/Ce1/Li1)O_{10}$ and $(Ca2/Sr2/Ce2/Li2)O_9$ with increasing $(Al/Si)O_4$ tetrahedra size. The arrows show how the structure changes with increasing Al concentration, x. The angles of O–(Ca/Sr/Ce/Li)–O, marked by orange sectors, increase with increasing x.

The average bond lengths $d(Ca1/Sr1–O)_{x=0}$ = 2.73(3) Å, $d(Ca1/Sr1–O)_{x=0.01}$ = 2.73(3) Å and $d(Ca1/Sr1–O)_{x=0.1}$ = 2.76(3) Å are bigger than $d(Ca2/Sr2–O)_{x=0}$ = 2.54(3) Å, $d(Ca2/Sr2–O)_{x=0.01}$ = 2.54(3) Å and $d(Ca2/Sr2–O)_{x=0.1}$ = 2.53(3) Å for compounds with x = 0, x = 0.01 and x = 0.1, respectively. The bigger coordination

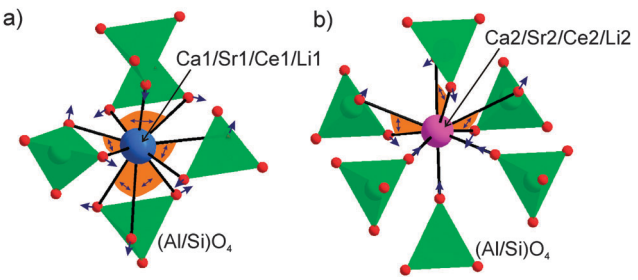

Fig. 6 Mechanism of the distortion polyhedra: (a) $(Ca1/Sr1/Ce1/Li1)O_{10}$ and (b) $(Ca2/Sr2/Ce2/Li2)O_9$ with increasing the $(Al/Si)O_4$ tetrahedra size. The blue arrows show how the structure changes with increasing Al concentration, x. The O–(Ca/Sr/Ce/Li)–O angles, which increase with x, are marked by orange sectors.

number of the Ca1/Sr1 site in comparison to the Ca2/Sr2 site should be the reason for this. This fact proves that the Sr ion is more likely to be located in a Ca1/Sr1 site. As a result, increasing the value of x from 0 to 0.1 did not lead to a drastic change in the Ca1/Sr1 or Ca2/Sr2 concentration and average bond lengths. The polyhedra distortion can be calculated by using the following formula:[29]

$$D = \frac{1}{n}\sum_{i=1}^{n}\frac{l_i - l_{av}}{l_{av}} \quad (8)$$

where l_i is the distance from the central atom to the ith coordinating atom, and l_{av} is the average bond length. The calculated results showed that the value of $D(Ca1/Sr1)_{x=0.1}$ = 0.076 is

bigger than that of $D(Ca1/Sr1)_{x=0.01}$ = 0.075 and $D(Ca1/Sr1)_{x=0}$ = 0.074 for the samples with x = 0.1, x = 0.01 and x = 0, respectively. The value of $D(Ca2/Sr2)_{x=0}$ = 0.033 for x = 0 also increases up to $D(Ca2/Sr2)_{x=0.01}$ = 0.041 and $D(Ca2/Sr2)_{x=0.1}$ = 0.048 for compounds with x = 0.01 and x = 0.1, respectively. Therefore, we can draw the conclusion that the increase in the distortion of the $(Ca1/Sr1/Ce1/Li1)O_{10}$ and $(Ca2/Sr2/Ce2/Li2)O_9$ polyhedra with increasing x is the reason for the red shift in these compounds.[30]

4. Conclusions

The effects of Al/Si substitution on the phase structures and luminescence properties of $CaSrSi_{1-x}Al_xO_4:Ce^{3+},Li^+$ phosphors were investigated in detail. The crystal structures were invariable when the doping amount of Al was below x = 0.1. The PL spectra showed that when the value x increases from 0 to 0.1, the emission spectra become gradually red shifted. The crystal structures of the $CaSrSi_{1-x}Al_xO_4:Ce^{3+},Li^+$ phosphors consist of disordered $(Si,Al)O_4$ tetrahedra and two types of cation polyhedra: $(Ca1/Sr1/Ce1/Li1)O_{10}$ and $(Ca2/Sr2/Ce2/Li2)O_9$. The increasing distortion of the $(Ca1/Sr1/Ce1/Li1)O_{10}$ and $(Ca2/Sr2/Ce2/Li2)O_9$ polyhedra with increasing x is the reason for the red shift. This result provides an impetus for the search for new phosphor hosts and explains the mechanism causing the red shift.

Acknowledgements

The present work was supported by the National Natural Science Foundations of China (Grant No. 51002146, 51272242), Natural Science Foundations of Beijing (2132050), the Program for New Century Excellent Talents in the University of the Ministry of Education of China (NCET-12-0950), Beijing Nova Program (Z131103000413047), Beijing Youth Excellent Talent Program (YETP0635), the Funds of the State Key Laboratory of New Ceramics and Fine Processing, Tsinghua University (KF201306) and the excellent tutor section of the Fundamental Research Funds for the Central Universities of China University of Geosciences, Beijing (2652015027).

References

1 S. Nakamura, M. Senoh and T. Mukai, *Appl. Phys. Lett.*, 1993, **62**, 2390–2392.
2 Z. G. Xia, Y. Y. Zhang, M. Molokeev, V. V. Atuchin and Y. Luo, *Sci. Rep.*, 2013, **3**, 3310.
3 A. Kalaji, M. Mikami and A. K. Cheetham, *Chem. Mater.*, 2014, **26**, 3966–3975.
4 F. W. Kang, Y. Zhang, L. Wondraczek, J. Q. Zhu, X. B. Yang and M. Y. Peng, *J. Mater. Chem. C*, 2014, **2**, 9850–9857.
5 Z. Y. Hou, C. X. Li, J. Yang, H. Z. Lian, P. P. Yang, R. Chai, Z. Y. Cheng and J. Lin, *J. Mater. Chem.*, 2009, **19**, 2737–2746.
6 F. W. Kang and M. Y. Peng, *Dalton Trans.*, 2014, **43**, 277–284.
7 Y. Y. Li, Q. S. Wu, X. C. Wang, J. Y. Ding, Q. Long and Y. H. Wang, *RSC Adv.*, 2014, **4**, 63569–63575.
8 Y. Chen, Y. Li, J. Wang, M. M. Wu and C. X. Wang, *J. Phys. Chem. C*, 2014, **118**, 12494–12499.
9 Z. D. Hao, J. H. Zhang, X. Zhang, Y. S. Luo, L. G. Zhang and H. F. Zhao, *J. Lumin.*, 2014, **152**, 40–43.
10 L. C. Ju, X. Xu, L. Y. Hao, Y. Lin and M. H. Lee, *J. Mater. Chem. C*, 2015, **3**, 1567–1575.
11 J. Park, S. J. Lee and Y. J. Kim, *Cryst. Growth Des.*, 2013, **13**, 5204–5210.
12 A. P. Black, K. A. Denault, J. Ora-Sole, A. R. Goni and A. Fuertes, *Chem. Commun.*, 2015, **51**, 2166–2169.
13 W. Z. Lv, M. M. Jiao, Q. Zhao, B. Q. Shao, W. Lv and H. P. You, *Inorg. Chem.*, 2014, **53**, 11007–11014.
14 S. H. Miao, Z. G. Xia, J. Zhang and Q. L. Liu, *Inorg. Chem.*, 2014, **53**, 10386–10393.
15 K. A. Denault, J. Brgoch, M. W. Gaultois, A. Mikhailovsky, R. Petry, H. Winkler, S. P. DenBaars and R. Seshadri, *Chem. Mater.*, 2014, **26**, 2275–2282.
16 M. Catti, G. Gazzoni and G. Ivaldi, *Acta Crystallogr., Sect. B: Struct. Crystallogr. Cryst. Chem.*, 1984, **40**, 537–544.
17 L. G. Van Uitert, *J. Lumin.*, 1984, **29**, 1.
18 J. L. Zhang, W. L. Zhang, Y. A. He, W. L. Zhou, L. P. Yu, S. X. Lian, Z. Q. Li and M. L. Gong, *Ceram. Int.*, 2014, **40**, 9831–9834.
19 Y. A. He, J. L. Zhang, W. L. Zhou, J. Han, Z. X. Qiu, L. P. Yu, C. Y. Rong and S. X. Lian, *J. Am. Ceram. Soc.*, 2014, **97**, 1517–1522.
20 G. Blasse, *Philips Res. Rep.*, 1969, **24**, 131–144.
21 H. H. Lin, G. B. Zhang, P. A. Tanner and H. B. Liang, *J. Phys. Chem. C*, 2013, **117**, 12769–12777.
22 L. L. Zhang, J. H. Zhang, X. Zhang, Z. D. Hao, H. F. Zhao and Y. S. Luo, *ACS Appl. Mater. Interfaces*, 2013, **5**, 12839–12846.
23 L. G. Van Uitert, *J. Electrochem. Soc.*, 1967, **114**, 1048.
24 R. J. Xie and N. Hirosaki, *Appl. Phys. Lett.*, 2007, **90**, 191101.
25 G. G. Li, Y. Zhang, D. L. Geng, M. M. Shang, C. Peng, Z. Y. Cheng and J. Lin, *ACS Appl. Mater. Interfaces*, 2012, **4**, 296–305.
26 T. Chengaiah, C. K. Jayasankar and L. R. Moorthy, *Physica B*, 2013, **431**, 137–141.
27 Z. G. Xia and W. W Wu, *Dalton Trans.*, 2013, **42**, 12989–12997.
28 Z. G. Xia and R. S. Liu, *J. Phys. Chem. C*, 2012, **116**, 15604.
29 K. A. Denault, N. C. George, S. R. Paden, S. Brinkley, A. A. Mikhailovsky, J. Neuefeind, S. P. DenBaars and R. Seshadri, *J. Mater. Chem.*, 2012, **22**, 18204–18213.
30 W. H. Baur, *Acta Crystallogr., Sect. B: Struct. Crystallogr. Cryst. Chem.*, 1974, **30**, 1195–1215.

